

LASER MEDICINE

https://doi.org/10.1070/QEL17300

Line curvature algorithm in laser ektacytometry of red blood cells

S.Yu. Nikitin, V.D. Ustinov, S.D. Shishkin, M.S. Lebedeva

Abstract. **The iso-intensity line curvature algorithm in laser ektacytometry of red blood cells is investigated by numerical simulation. The algorithm is designed to measure the average deformability, as well as the width and asymmetry of the red blood cell deformability distribution in a blood sample under study. The accuracy and scope of the algorithm are determined. Using a bimodal ensemble as an example, the possibility of determining the fraction of weakly deformable red blood cells in a blood sample by laser ektacytometry is demonstrated.**

Keywords: *deformability of red blood cells, laser diffractometry, erythrocyte deformability distribution.*

1. Introduction

Ektacytometry is a blood test designed to measure the deformability of red blood cells, i.e. the ability of blood cells to change their shape under the influence of external forces. Measurement of this parameter is important for assessing the general state of the human body, as well as for the diagnosis and treatment of diseases such as sickle cell anaemia [1–3], malaria [4], ischemia [5], and many others [6, 7]. In a laser ektacytometer, a suspension of red blood cells deformed by viscous friction forces is illuminated with a laser beam. In this case, a light scattering pattern is observed in the far diffraction zone, which contains information about the shapes of blood cells in a given shear stress field. The task of the theory is to relate the parameters of the observed diffraction pattern with the characteristics of the red blood cell ensemble. Algorithms for processing laser ektacytometry data are constructed on this basis.

The analysis of the diffraction pattern is carried out on the basis of the concept of an iso-intensity line. This is the name of the line on the observation screen, on which the intensity of the scattered light has a certain constant value. For normal blood samples, the iso-intensity line looks like an ellipse. The appearance of a fraction of hard cells in the human blood leads to the fact that the iso-intensity line becomes diamond-shaped. This line shape is typical for the blood of patients with sickle cell anaemia [1].

In our works [8–15], we have proposed algorithms for processing laser ektacytometry data, which make it possible to measure population characteristics of a blood sample, such as average deformability, as well as width, asymmetry, and coefficient of kurtosis in the erythrocyte deformability distribution. The line curvature algorithm [10, 13] uses as input the coordinates of the polar points of the iso-intensity line and the parameters of the curvature of the line at these points.

For the practical application of the line curvature algorithm, it is required to evaluate its accuracy, as well as the area of its applicability both with respect to the permissible heterogeneity of the red blood cell ensemble and with respect to a fragment of the diffraction pattern suitable for measurements. In this paper, we use numerical simulation to test the line curvature algorithm under ideal conditions when the input data for it are specified exactly. Of particular interest is the possibility of measuring the fraction of weakly deformable red blood cells in a blood sample by laser ektacytometry. This issue is also considered in this work.

2. Laser ektacytometry of red blood cells

In a laser ektacytometer, a highly diluted suspension of red blood cells is poured into a thin gap between the walls of two transparent coaxial cups, one of which is stationary and the other can rotate at a given angular velocity (a so-called Couette cell) [16–19]. The rotation of the movable cup creates a uniform field of shear stresses in the suspension, which pulls the erythrocytes along the flow. The suspension is illuminated with a laser beam and the resulting light scattering pattern is observed. The optical layout of the ektacytometer is shown in Fig. 1. It includes a laser, a Couette cell, and a diffraction pattern observation screen.

To obtain a high-quality diffraction pattern, a highly coherent laser beam is required. An ektacytometer video cam-

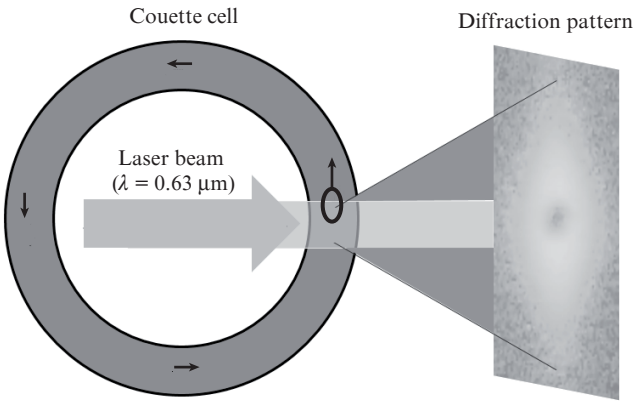

Figure 1. Optical layout of a laser ektacytometer of red blood cells.

S.Yu. Nikitin, V.D. Ustinov, S.D. Shishkin, M.S. Lebedeva Faculty of Physics and Faculty of Computational Mathematics and Cybernetics, Lomonosov Moscow State University, Vorob'evy Gory, 119991 Moscow, Russia; e-mail: sergeynikitin007@yandex.ru

Received 21 February 2020
Kvantovaya Elektronika **50** (9) 888–894 (2020)
Translated by I.A. Ulitkin

era recording a diffraction pattern must have a resolution of about 100 megapixels and a dynamic range of light intensity measurement of at least 50 [20].

2.1. Characteristics of the red blood cell ensemble

Following works [10, 13], red blood cells in the shear flow of a laser ektacytometer will be modelled by elliptical disks with semi-axes a and b. Taking into account the inhomogeneity of the ensemble in particle shapes, we will consider the semi-axes a and b as random variables and describe them by the formulae

$$a = a_0(1 + \varepsilon), \quad b = b_0(1 - \varepsilon).$$

Here a_0 and b_0 are the average sizes of the semi-axes; and ε is a random parameter, the average value of which is assumed to be zero:

$$\langle \varepsilon \rangle = 0. \tag{1}$$

The ensemble of red blood cells is characterised by parameters

$$s = \frac{a_0}{b_0}, \ \mu = \langle \varepsilon^2 \rangle, \ \nu = \langle \varepsilon^3 \rangle. \tag{2}$$

These parameters describe the average deformability, width and asymmetry of the erythrocyte deformability distribution.

2.2. Line curvature algorithm

The construction of an algorithm for processing laser ektacytometry data includes two main procedures. First, on the basis of a certain model of an ensemble of red blood cells, we solve the direct problem of scattering a laser beam by an ensemble of particles and calculate the parameters of the diffraction pattern to be measured. Then we solve the inverse scattering problem and express the desired characteristics of the red blood cell ensemble through the parameters of the diffraction pattern. The solution to the inverse scattering problem is approximate. It is possible on the basis of additional assumptions regarding the properties of the erythrocyte ensemble and the area of the diffraction pattern used for measurements. These assumptions make it possible to single out small parameters of the problem, linearise the diffractometric equations, and find their analytical solution. As a result, we obtain formulae expressing the desired characteristics of an ensemble of red blood celld through the parameters of the diffraction pattern.

The input data for the line curvature algorithm are the parameters of the diffraction pattern arising from the scattering of the laser beam by an erythrocyte suspension. These are such parameters as the normalised light intensity $\tilde{I}$ on the iso-intensity line selected for measurements, the coordinates of the polar points of this line $(x_p,0)$ and $(0,y_p)$, as well as the radii of its curvature $R(x_p,0) \equiv R(x_p)$ and $R(0,y_p) \equiv R(y_p)$ at the indicated points. Here we use a Cartesian coordinate system, the origin of which is located in the centre of the diffraction pattern (the point of incidence of a direct laser beam on the screen). The x axis is horizontal, and the y axis is vertical. One of them is parallel to the direction of the flow in the Couette cell, and the other is perpendicular to it. An example of a diffraction pattern, an iso-intensity line and circles of curvature of this line at polar points are shown in Fig. 2.

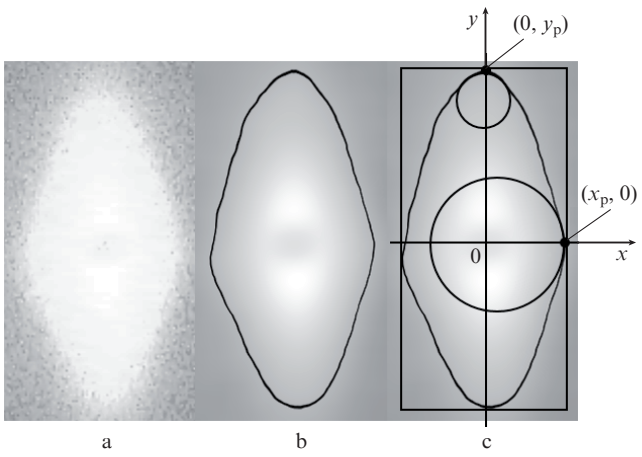

Figure 2. (a) Example of a diffraction pattern, (b) iso-intensity line, and (c) circles with radii $R(x_p,0)$ and $R(0,y_p)$ at polar points.

The line curvature algorithm is based on the use of formulae [13]

$$s = \frac{Q}{1 + \sqrt{1 - 2Qq C_1}}, \quad \mu = \frac{1}{2q_1}\left(\frac{C_2}{s} + C_1 s\right) - \frac{1}{q_1},$$
$$\nu = \frac{1}{2q_2}\left(\frac{C_2}{s} - C_1 s\right). \tag{3}$$

Here

$$C_1 = \sqrt{\frac{x_p}{R(x_p)}} = \sqrt{x_p \left| \frac{d^2 x}{dy^2}(y = 0) \right|}; \tag{4}$$
$$C_2 = \sqrt{\frac{y_p}{R(y_p)}} = \sqrt{y_p \left| \frac{d^2 y}{dx^2}(x = 0) \right|};$$

$$q = \frac{q_0}{2q_2}; \quad Q = 2(D - qC_2); \quad D = \frac{y_p}{x_p}; \tag{5}$$
$$q_0 = \frac{2}{\sqrt{f_0}}; \quad f_0 = \frac{1}{4\beta^2}\tilde{I}; \quad \tilde{I} = \frac{I}{I(0)}; \quad \beta = -0.4;$$

$$q_1 = 8 + q_0; \quad q_2 = 16 + 4q_0; \tag{6}$$

and I and $I(0)$ are the light intensities at the iso-intensity line and in the centre of the diffraction pattern, respectively. Our task is to evaluate the accuracy of formulae (3)–(6) and determine the area of their applicability. Let us make this estimate under the conditions when the input data for the line curvature algorithm are specified exactly. To this end, we use the model of a bimodal ensemble of red blood cells.

3. Bimodal ensemble of red blood cells

In the particular case of a bimodal (i.e., two-component) erythrocyte ensemble, the random parameter ε has only two possible values, i.e. ε_1 and ε_2. These values correspond to two types (shapes) of particles in the ensemble. The sizes of the semi-axes of the elliptical disks of the first and second types are determined by the expressions

$$a_1 = a_0(1+\varepsilon_1), \quad b_1 = b_0(1-\varepsilon_1),$$
$$a_2 = a_0(1+\varepsilon_2), \quad b_2 = b_0(1-\varepsilon_2). \tag{7}$$

Let p be the fraction of particles of the first type (hard cells) in the ensemble of red blood cells. Then, according to formulae (1) and (2),

$$p\varepsilon_1 + (1-p)\varepsilon_2 = 0, \ \mu = p\varepsilon_1^2 + (1-p)\varepsilon_2^2,$$
$$\nu = p\varepsilon_1^3 + (1-p)\varepsilon_2^3. \tag{8}$$

Shape parameters of bimodal ensemble components (aspect ratios) are expressed as

$$s_1 = \frac{a_1}{b_1}, \quad s_2 = \frac{a_2}{b_2}. \tag{9}$$

Without loss of generality, we will assume that $s_1 < s_2$, i.e., particles of the first type are more rigid than particles of the second type.

It follows from formulae (7)–(9) that

$$\varepsilon_1 = \frac{s_1 - s}{s_1 + s}, \quad \varepsilon_2 = \frac{s_2 - s}{s_2 + s}, \tag{10}$$

where

$$s = M + \sqrt{M^2 + s_1 s_2}; \quad M = (s_1 - s_2)(p - 1/2). \tag{11}$$

Thus, specifying the shapes of the components of the bimodal ensemble, s_1 and s_2, and the fraction of particles of the first type, p, we can calculate the parameters ε_1, ε_2, and s by formulae (10) and (11).

Solving equations (8) with respect to the quantities ε_1, ε_2, and p, we find the expressions

$$p = \frac{1}{2}\left(1 + \frac{\nu}{\sqrt{\nu^2 + 4\mu^3}}\right), \quad \varepsilon_1 = \frac{\nu - \sqrt{\nu^2 + 4\mu^3}}{2\mu},$$
$$\varepsilon_2 = \frac{\nu + \sqrt{\nu^2 + 4\mu^3}}{2\mu}. \tag{12}$$

It follows from equations (10) that

$$s_1 = s\frac{1+\varepsilon_1}{1-\varepsilon_1}, \quad s_2 = s\frac{1+\varepsilon_2}{1-\varepsilon_2}. \tag{13}$$

Thus, having determined the parameters s, μ, and ν using the line curvature algorithm, we can calculate the parameters of the bimodal ensemble p, s_1, and s_2 by formulae (12) and (13). This means that for a bimodal ensemble of red blood cels, laser ektacytometry makes it possible to determine the proportion of rigid cells p in the ensemble of erythrocytes and the cell shapes (aspect ratios) s_1 and s_2 of both components of the ensemble.

3.1. Scattering of a laser beam by a bimodal ensemble of red blood cells

Let us estimate the accuracy of measuring the parameters of a bimodal erythrocyte ensemble using the line curvature algorithm. Let us consider the scattering of a laser beam by an ensemble of elliptical disks located in a certain plane perpendicular to the laser beam. We will assume that the major axes of the ellipses are parallel to each other, and the centres of the disks are randomly distributed in the indicated plane. In this case, the distribution of the light intensity in the far diffraction zone is described by the formula [8]

$$I = \frac{1}{4} I_0 N |\gamma|^2 \left\langle \left(ab\frac{k}{z}\right)^2 G(\xi) \right\rangle. \tag{14}$$

Here, angle brackets denote averaging over parameters a and b;

$$\xi = \xi(x,y) = \frac{k}{z}\sqrt{a^2x^2 + b^2y^2}; \quad G(\xi) = \left[\frac{2J_1(\xi)}{\xi}\right]^2;$$
$$G'(\xi) = \frac{\mathrm{d}G}{\mathrm{d}\xi} = \frac{8}{\xi^3}[\xi J_0(\xi) - 2J_1(\xi)]J_1(\xi); \tag{15}$$

x, y are the Cartesian coordinates of a point on the observation screen in the coordinate system, the origin of which is at the centre of the diffraction pattern; I_0 is the intensity of the incident laser beam; N is the number of particles illuminated by the laser beam; z is the distance from the measurement volume to the observation screen; $k = 2\pi/\lambda$ is the wave number; λ is the wavelength of the light; and $J_0(x)$ and $J_1(x)$ are the Bessel functions of the zero and first orders, respectively. The parameter $|\gamma|^2$ is determined by the thickness and optical density of the disk. The function $G(\xi)$ satisfies the condition $G(0) = 1$. Note that formula (14) describes the distribution of the light intensity at those points of the observation screen where the direct laser beam does not fall.

In particular, for a bimodal ensemble of red blood cells with characteristics a_1, b_1 and a_2, b_2, as well as the fractions p of particles of the first type, we obtain the expression

$$I = \frac{1}{4} I_0 N |\gamma|^2 \times \left[p\left(a_1 b_1 \frac{k}{z}\right)^2 G(\xi_1) + (1-p)\left(a_2 b_2 \frac{k}{z}\right)^2 G(\xi_2)\right],$$

where

$$\xi_1 = \frac{k}{z}\sqrt{a_1^2x^2 + b_1^2y^2}; \quad \xi_2 = \frac{k}{z}\sqrt{a_2^2x^2 + b_2^2y^2}. \tag{16}$$

Light intensity at the centre of the diffraction pattern is expressed as

$$I(0) = \frac{1}{4} I_0 N |\gamma|^2 \left[p\left(a_1 b_1 \frac{k}{z}\right)^2 + (1-p)\left(a_2 b_2 \frac{k}{z}\right)^2\right].$$

The normalised intensity has the form

$$\tilde{I} = \tilde{I}(x,y) = \frac{I}{I(0)} = \frac{p(a_1b_1)^2 G(\xi_1) + (1-p)(a_2b_2)^2 G(\xi_2)}{p(a_1b_1)^2 + (1-p)(a_2b_2)^2}. \tag{17}$$

Formulae (16) and (17) describe the distribution of the light intensity in the diffraction pattern arising from the scattering of a laser beam by a bimodal (in shape) ensemble of particles.

3.2. Iso-intensity line

The intensity of the scattered light on the iso-intensity line has a certain constant value:

$$\tilde{I} = \text{const}. \tag{18}$$

Formulae (16)–(18) implicitly define the function $x = x(y)$ or $y = y(x)$, which describes the shape of the iso-intensity line. The points of intersection of the iso-intensity line with the Cartesian coordinate axes are called polar. We are interested in the ratio of the coordinates of the polar points $D = y_p/x_p$, as well as in the curvature parameters C_1 and C_2 of the iso-intensity line at these points.

To normalise the coordinates, we introduce the parameter $c_0 = \sqrt{a_0 b_0}$, which characterises the average size of a red blood cell, as well as the dimensionless quantities U and V, determined by the formulae

$$U = \sqrt{s}\,\frac{k}{z}\,c_0 x, \quad V = \frac{1}{\sqrt{s}}\,\frac{k}{z} c_0 y.$$

In these variables, the iso-intensity line is described by the function $U(V)$ or $V(U)$, and its parameters take the form

$$D = s\frac{V(0)}{U(0)}, C_1 = \frac{1}{s}\sqrt{|\,U(0)\,U''(0)\,|}, C_2 = s\sqrt{|\,V(0)\,V''(0)\,|}. \quad (19)$$

The iso-intensity line shape is determined by the equation

$$\tilde{I} = \tilde{I}(U,V) = \frac{p(1-\varepsilon_1^2)^2 G(\xi_1) + (1-p)(1-\varepsilon_2^2)^2 G(\xi_2)}{p(1-\varepsilon_1^2)^2 + (1-p)(1-\varepsilon_2^2)^2} = \text{const}$$

or the equation

$$p(1-\varepsilon_1^2)^2 G(\xi_1) + (1-p)(1-\varepsilon_2^2)^2 G(\xi_2) = \text{const}, \quad (20)$$

where

$$\xi_1 = \sqrt{(1+\varepsilon_1)^2 U^2 + (1-\varepsilon_1)^2 V^2}; \qquad \xi_2 = \sqrt{(1+\varepsilon_2)^2 U^2 + (1-\varepsilon_2)^2 V^2}. \quad (21)$$

For the normalised coordinates of the polar points $U_p = U(0)$ and $V_p = V(0)$, we obtain the transcendental equations

$$\tilde{I} = \frac{p(1-\varepsilon_1^2)^2 G[(1+\varepsilon_1)\,U_p] + (1-p)(1-\varepsilon_2^2)^2 G[(1+\varepsilon_2)\,U_p]}{p(1-\varepsilon_1^2)^2 + (1-p)(1-\varepsilon_2^2)^2}, \quad (22)$$

$$\tilde{I} = \frac{p(1-\varepsilon_1^2)^2 G[(1-\varepsilon_1)\,V_p] + (1-p)(1-\varepsilon_2^2)^2 G[(1-\varepsilon_2)\,V_p]}{p(1-\varepsilon_1^2)^2 + (1-p)(1-\varepsilon_2^2)^2}, \quad (23)$$

where the function G is defined by formula (15).

3.3. Iso-intensity line curvature parameters

Let us calculate the curvature parameter C_2 of the iso-intensity line at the upper polar point. To this end, we use formulae (20) and (21), in which we will consider the variable V as a function of the variable U. Differentiating equality (20) with respect to U, we obtain

$$p(1-\varepsilon_1^2)^2 G'(\xi_1)\frac{d\xi_1}{dU} + (1-p)(1-\varepsilon_2^2)^2 G'(\xi_2)\frac{d\xi_2}{dU} = 0, \quad (24)$$

where

$$\frac{d\xi_1}{dU} = \frac{(1+\varepsilon_1)^2 U + (1-\varepsilon_1)^2 VV'}{\xi_1}; \qquad \frac{d\xi_2}{dU} = \frac{(1+\varepsilon_2)^2 U + (1-\varepsilon_2)^2 VV'}{\xi_2}; \; V' = \frac{dV}{dU}.$$

In particular, for $U = 0$ we have

$$p(1-\varepsilon_1^2)^2 G'(\xi_{10})\frac{d\xi_1}{dU}\Big|_{U=0} + (1-p)(1-\varepsilon_2^2)^2 G'(\xi_{20})\frac{d\xi_2}{dU}\Big|_{U=0} = 0, \quad (25)$$

$$\frac{d\xi_1}{dU}\Big|_{U=0} = \frac{(1-\varepsilon_1)^2 V(0)\,V'(0)}{\xi_{10}} = \frac{(1-\varepsilon_1)^2 V(0)\,V'(0)}{(1-\varepsilon_1)\,V(0)} = (1-\varepsilon_1)\,V'(0), \quad (26)$$

$$\frac{d\xi_2}{dU}\Big|_{U=0} = \frac{(1-\varepsilon_2)^2 V(0)\,V'(0)}{\xi_{20}} = \frac{(1-\varepsilon_2)^2 V(0)\,V'(0)}{(1-\varepsilon_2)\,V(0)} = (1-\varepsilon_2)\,V'(0), \quad (27)$$

where

$$\xi_{10} = \xi_1(U=0) = (1-\varepsilon_1)\,V(0); \qquad \xi_{20} = \xi_2(U=0) = (1-\varepsilon_2)\,V(0). \quad (28)$$

It follows from (25)–(27) that

$$V'(U=0) = 0, \quad \frac{d\xi_1}{dU}\Big|_{U=0} = 0, \quad \frac{d\xi_2}{dU}\Big|_{U=0} = 0. \quad (29)$$

Now we differentiate equality (24) with respect to U and obtain

$$p(1-\varepsilon_1^2)^2\left[G''(\xi_1)\left(\frac{d\xi_1}{dU}\right)^2 + G'(\xi_1)\frac{d^2\xi_1}{dU^2}\right] + (1-p)(1-\varepsilon_2^2)^2\left[G''(\xi_2)\left(\frac{d\xi_2}{dU}\right)^2 + G'(\xi_2)\frac{d^2\xi_2}{dU^2}\right] = 0.$$

Setting here $U = 0$ and taking formulae (29) into account, we have

$$p(1-\varepsilon_1^2)^2 G'(\xi_{10})\frac{d^2\xi_1}{dU^2}\Big|_{U=0} + (1-p)(1-\varepsilon_2^2)^2 G'(\xi_{20})\frac{d^2\xi_2}{dU^2}\Big|_{U=0} = 0, \quad (30)$$

where

$$\frac{d^2\xi_1}{dU^2} = \frac{d}{dU}\left[\frac{(1+\varepsilon_1)^2 U + (1-\varepsilon_1)^2 VV'}{\xi_1}\right]; \qquad \frac{d^2\xi_2}{dU^2} = \frac{d}{dU}\left[\frac{(1+\varepsilon_2)^2 U + (1-\varepsilon_2)^2 VV'}{\xi_2}\right]$$

or

$$\frac{d^2\xi_1}{dU^2} = \frac{1}{\xi_1}\frac{d}{dU}[(1+\varepsilon_1)^2 U + (1-\varepsilon_1)^2 VV'] - [(1+\varepsilon_1)^2 U + (1-\varepsilon_1)^2 VV']\frac{1}{\xi_1^2}\frac{d\xi_1}{dU},$$

$$\frac{d^2\xi_2}{dU^2} = \frac{1}{\xi_2}\frac{d}{dU}[(1+\varepsilon_2)^2 U + (1-\varepsilon_2)^2 VV'] - [(1+\varepsilon_2)^2 U + (1-\varepsilon_2)^2 VV']\frac{1}{\xi_2^2}\frac{d\xi_2}{dU}.$$

Setting here $U = 0$ and taking (29) into account, we obtain

$$\left.\frac{d^2\xi_1}{dU^2}\right|_{U=0} = \frac{(1+\varepsilon_1)^2 + (1-\varepsilon_1)^2[V'(0)V'(0) + V(0)V''(0)]}{\xi_{10}},$$

$$\left.\frac{d^2\xi_2}{dU^2}\right|_{U=0} = \frac{(1+\varepsilon_2)^2 + (1-\varepsilon_2)^2[V'(0)V'(0) + V(0)V''(0)]}{\xi_{20}}$$

or

$$\left.\frac{d^2\xi_1}{dU^2}\right|_{U=0} = \frac{(1+\varepsilon_1)^2 + (1-\varepsilon_1)^2 V(0)V''(0)}{\xi_{10}},$$

$$\left.\frac{d^2\xi_2}{dU^2}\right|_{U=0} = \frac{(1+\varepsilon_2)^2 + (1-\varepsilon_2)^2 V(0)V''(0)}{\xi_{20}}.$$

Substituting these expressions into formula (30), we find

$$p(1-\varepsilon_1^2)^2 G'(\xi_{10})\frac{(1+\varepsilon_1)^2 + (1-\varepsilon_1)^2 V(0)V''(0)}{\xi_{10}} + (1-p)(1-\varepsilon_2^2)^2 G'(\xi_{20})\frac{(1+\varepsilon_2)^2 + (1-\varepsilon_2)^2 V(0)V''(0)}{\xi_{20}} = 0.$$

Thus,

$$V(0)V''(0) = -\frac{p(1-\varepsilon_1^2)^2 G'(\xi_{10})\frac{(1+\varepsilon_1)^2}{\xi_{10}} + (1-p)(1-\varepsilon_2^2)^2 G'(\xi_{20})\frac{(1+\varepsilon_2)^2}{\xi_{20}}}{p(1-\varepsilon_1^2)^2 G'(\xi_{10})\frac{(1-\varepsilon_1)^2}{\xi_{10}} + (1-p)(1-\varepsilon_2^2)^2 G'(\xi_{20})\frac{(1-\varepsilon_2)^2}{\xi_{20}}}. \quad (31)$$

Here, ξ_{10} and ξ_{20} are determined by formulae (28). Substituting (31) into formula (19) for C_2, we obtain

$$C_2 = s\sqrt{\frac{g_{1V}G'[(1-\varepsilon_1)V_p] + g_{2V}G'[(1-\varepsilon_2)V_p]}{h_{1V}G'[(1-\varepsilon_1)V_p] + h_{2V}G'[(1-\varepsilon_2)V_p]}}, \quad (32)$$

where

$$g_{1V} = (1-\varepsilon_1)(1+\varepsilon_1)^4 p; \quad g_{2V} = (1-\varepsilon_2)(1+\varepsilon_2)^4(1-p);$$
$$h_{1V} = (1-\varepsilon_1)^3(1+\varepsilon_1)^2 p; \quad h_{2V} = (1-\varepsilon_2)^3(1+\varepsilon_2)^2(1-p). \quad (33)$$

Similarly, we find the parameter of the curvature of the iso-intensity line for the right polar point:

$$C_1 = \frac{1}{s}\sqrt{\frac{g_{1U}G'[(1+\varepsilon_1)U_p] + g_{2U}G'[(1+\varepsilon_2)U_p]}{h_{1U}G'[(1+\varepsilon_1)U_p] + h_{2U}G'[(1+\varepsilon_2)U_p]}}, \quad (34)$$

where

$$g_{1U} = (1-\varepsilon_1)^4(1+\varepsilon_1)p; \quad g_{2U} = (1-\varepsilon_2)^4(1+\varepsilon_2)(1-p);$$
$$h_{1U} = (1-\varepsilon_1)^2(1+\varepsilon_1)^3 p; \quad h_{2U} = (1-\varepsilon_2)^2(1+\varepsilon_2)^3(1-p). \quad (35)$$

The function G' in expressions (32) and (34) is defined by formula (15).

4. Testing the algorithm

The test procedure for the line curvature algorithm is as follows. Setting the parameters of the bimodal ensemble of erythrocytes s_1, s_2, and p, we calculate the parameters ε_1, ε_2, and s by formulae (10) and (11). Then we determine the parameters D, C_1, and C_2 by formulae (19), (22), (23), and (32)–(35). After that, setting the parameter $\tilde{I}$ and using the line curvature algorithm, we find the parameters s, μ, and v by formulae (3)–(6). Finally, using formulae (12) and (13), we determine the parameters s_1, s_2, and p. In these calculations, only formulae (3)–(6) are approximate. The rest of the formulae in the framework of the adopted model of light scattering by red blood cells are accurate. Therefore, comparing the obtained values of s_1, s_2, and p with the initially specified ones, we will be able to estimate the accuracy of formulae (3)–(6) describing the line curvature algorithm.

4.1. Calculation results

We have performed numerical calculations for the following parameter values:

$$s_1 = 1, \ 1.5 \leqslant s_2 \leqslant 2.5, \ 0.02 \leqslant \tilde{I} \leqslant 0.2, \ 0.1 \leqslant p \leqslant 0.9.$$

In this case, the parameter s_2 changed with a step of 0.25; the parameter p, with a step of 0.1; and the parameter $\tilde{I}$, with a step of 0.005. Then the initially set values of s_1, s_2, and p were compared with those calculated using formulae (3)–(6).

The calculation results are presented in Table 1. It indicates the ranges of parameter values for which the line curvature algorithm determined the characteristics of a bimodal erythrocyte ensemble with an error of less than 10%. The obtained data show that, for certain values of the parameters, the line curvature algorithm provides measurement accuracy sufficient for practical applications.

It can be seen from Table 1 that, for a symmetric ensemble of red blood cells, when $p = 0.5$, the line curvature algorithm works well over the entire investigated range of variation of the parameter $\tilde{I}$, from 0.02 to 0.2. In this case, the error in determining the parameters s_1, s_2, and p using the line curvature algorithm does not exceed 10%. If the ensemble of erythrocytes is asymmetric, i.e. $p \neq 0.5$, then the permissible values of the parameter $\tilde{I}$ do not exceed 0.12. For strongly asymmetric ensembles of red blood cells, when $p = 0.1$ or 0.9, the aspect ratio for a soft particle (parameter s_2) can be measured with an error of less than 10% only for the range of values $1.5 \leqslant s_2 \leqslant 2.25$.

Table 1. Data obtained by numerical simulation.

Fraction of rigid cells p	Aspect ratio s_2	Normalised intensity $\tilde{I}$
0.1	$1.5 \leqslant s_2 \leqslant 2.25$	$0.02 \leqslant \tilde{I} \leqslant 0.025$
0.2	1.5	$0.025 \leqslant \tilde{I} \leqslant 0.03$
0.2	1.75	$0.035 \leqslant \tilde{I} \leqslant 0.04$
0.2	2.0	$0.035 \leqslant \tilde{I} \leqslant 0.04$
0.2	2.25	$0.04 \leqslant \tilde{I} \leqslant 0.045$
0.2	2.5	$0.045 \leqslant \tilde{I} \leqslant 0.05$
0.3	1.5	$0.025 \leqslant \tilde{I} \leqslant 0.04$
0.3	1.75	$0.03 \leqslant \tilde{I} \leqslant 0.05$
0.3	2.0	$0.04 \leqslant \tilde{I} \leqslant 0.06$
0.3	2.25	$0.05 \leqslant \tilde{I} \leqslant 0.07$
0.3	2.5	$0.06 \leqslant \tilde{I} \leqslant 0.08$
0.4	1.5	$0.02 \leqslant \tilde{I} \leqslant 0.065$
0.4	1.75	$0.025 \leqslant \tilde{I} \leqslant 0.075$
0.4	2.0	$0.04 \leqslant \tilde{I} \leqslant 0.09$
0.4	2.25	$0.05 \leqslant \tilde{I} \leqslant 0.1$
0.4	2.5	$0.065 \leqslant \tilde{I} \leqslant 0.115$
0.5	$1.5 \leqslant s_2 \leqslant 2.5$	$0.02 \leqslant \tilde{I} \leqslant 0.2$
0.6	1.5	$0.02 \leqslant \tilde{I} \leqslant 0.08$
0.6	1.75	$0.02 \leqslant \tilde{I} \leqslant 0.095$
0.6	2.0	$0.03 \leqslant \tilde{I} \leqslant 0.105$
0.6	2.25	$0.045 \leqslant \tilde{I} \leqslant 0.12$
0.6	2.5	$0.055 \leqslant \tilde{I} \leqslant 0.115$
0.7	1.5	$0.02 \leqslant \tilde{I} \leqslant 0.055$
0.7	1.75	$0.02 \leqslant \tilde{I} \leqslant 0.065$
0.7	2.0	$0.025 \leqslant \tilde{I} \leqslant 0.075$
0.7	2.25	$0.035 \leqslant \tilde{I} \leqslant 0.075$
0.7	2.5	$0.05 \leqslant \tilde{I} \leqslant 0.075$
0.8	1.5	$0.02 \leqslant \tilde{I} \leqslant 0.05$
0.8	1.75	$0.02 \leqslant \tilde{I} \leqslant 0.045$
0.8	2.0	$0.025 \leqslant \tilde{I} \leqslant 0.045$
0.8	2.25	$0.03 \leqslant \tilde{I} \leqslant 0.045$
0.8	2.5	$0.04 \leqslant \tilde{I} \leqslant 0.045$
0.9	1.5	$0.02 \leqslant \tilde{I} \leqslant 0.035$
0.9	1.75	$0.02 \leqslant \tilde{I} \leqslant 0.03$
0.9	2.0	$0.02 \leqslant \tilde{I} \leqslant 0.025$
0.9	2.25	0.02

4.2. Discussion of the results

In this work, we have tested the algorithm for processing erythrocyte laser ektacytometry data, designed to determine the parameters of erythrocyte deformability distribution. Relying on the analysis of the diffraction pattern that occurs when a laser beam is scattered by an ensemble of blood cells deformed by viscous friction forces, the line curvature algorithm determines three population characteristics of a blood sample, namely, the average deformability of erythrocytes, as well as the width and asymmetry of their deformability distribution. In the particular case of a bimodal ensemble, these data are sufficient to determine the proportion of hard erythrocytes in a blood sample, as well as the shape (aspect ratio) of both components of the ensemble. Regarding our assumption that the bimodal ensemble of red blood cells contains rigid (non-deformable) cells, we note that these cells are indeed present in human blood in diseases such as hereditary spherocytosis, sickle cell anaemia, and malaria. In addition, we plan to test the line curvature algorithm on specially prepared blood samples, when some of the cells are treated with a glutaraldehyde solution.

We have tested the operation of the line curvature algorithm under ideal conditions, when the input data for the algorithm are precisely specified. The verification has been performed by the method of numerical simulation for a bimodal ensemble of red blood cells with a rigid cell component. The region of applicability of the algorithm is found, for which the error in determining the parameters of the bimodal ensemble does not exceed 10%.

The calculation results show that the highest measurement accuracy is achieved for a symmetric ensemble of cells when both components of the ensemble (soft and hard erythrocytes) are represented in equal amounts. In this case, a wide area of the diffraction pattern is suitable for measurements, within which the intensity of the scattered light on the iso-intensity line is 2%–20% of the intensity of the central diffraction maximum. For strongly asymmetric ensembles, when the fraction of one of the ensemble components is 10%, only a narrow region of the diffraction pattern is suitable for the analysis, within which the intensity of the scattered light on the iso-intensity line is 2%–3% of the intensity of the central diffraction maximum. Another limitation is associated with the fact that high measurement accuracy is achieved only for weakly inhomogeneous ensembles of red blood cells, when the aspect ratio for the soft component of the ensemble does not exceed 2.25. This, in turn, imposes a limitation on the permissible value of the shear stress acting on blood cells in the shear flow of the laser ektacytometer.

5. Conclusions

Using the numerical simulation method, we have tested the line curvature algorithm designed to measure the average deformability of red blood cells, as well as the width and asymmetry of their deformability distribution. It is shown that this algorithm provides a measurement accuracy sufficient for practical applications. In particular, it allows one to measure the proportion of weakly deformable erythrocytes in a test blood sample. The highest measurement accuracy is achieved when the peripheral part of the diffraction pattern is used for the analysis, where the light intensity is 5%–10% of the intensity of the central diffraction maximum. As for the shear stress acting on blood cells in the shear flow of the ektacytometer, optimal operation of the algorithm is expected when it does not exceed the value at which the deformation of normal blood cells is characterised by an aspect ratio (length to width ratio) of 2.5. The data obtained will be used in the design and development of an improved model of a laser ektacytometer of red blood cells.

Acknowledgements. The authors are grateful to A.V. Priezzhev for a discussion of the results of this work and useful comments.

This work was supported by the Russian Science Foundation (Grant No. 18-71-00158).

References

1. Renoux C., Parrow N., Faes C., et al. *Clin. Hemorheol. Microcircul.*, **62**, 173 (2016). DOI: 10.3233/CH-151979.
2. Rabai M., Detterich J.A., Wenby R.B., et al. *Biorheology*, **51**, 159 (2014). DOI: 10.3233/BIR-140660.
3. Rab M.A.E., van Oirschot B.A., Bos J., et al. *Am. J. Hematol.*, **94** (5), 575 (2019). DOI: 10.1002/ajh.25443.
4. Dondorp A.M. *On the Pathophysiology of Severe Falciparum Malaria with Special Reference to Red Cell Deformability* (Amsterdam: Thela Thesis, 1999).
5. Azhermacheva M.N., Plotnikov D.M., Aliev O.I., et al. *Bullutin of Siberian Medicine*, **12** (5), 5 (2013); https://doi.org/10.20538/1682-0363-2013-5-5-12.
6. Toth K., Kesmarky G., Alexy T., in *Handbook of Hemorheology and Hemodynamics* (Amsterdam: IOS Press, 2007).
7. Murav'ev A.V., Tikhomirova I.A., Bulaeva S.V., Petrochenko E.P. *Reologicheskie svoistva krovi pri lechenii zlokachestvennykh opukholei, ateroskleroza i diabeta* (Rheological Properties of Blood in the Treatment of Malignant Tumours, Atherosclerosis and Diabetes) (Yaroslavl: Kantsler Publ. House, 2016).
8. Nikitin S.Yu., Priezzhev A.V., Lugovtsov A.E. *J. Quant. Spectrosc. Radiat. Transfer*, **121**, 1 (2013).
9. Nikitin S.Yu., Priezzhev A.V., Lugovtsov A.E., Ustinov V.D. *Quantum Electron.*, **44** (8), 774 (2014) [*Kvantovaya Elektron.*, **44** (8), 774 (2014)].
10. Nikitin S.Yu., Priezzhev A.V., Lugovtsov A.E., Ustinov V.D., Razgulin A.V. *J. Quant. Spectrosc. Radiat. Transfer*, **146**, 365 (2014).
11. Nikitin S.Yu., Yurchuk Yu.S. *Quantum Electron.*, **45** (8), 776 (2015) [*Kvantovaya Elektron.*, **45** (8), 776 (2015)].
12. Nikitin S.Yu., Ustinov V.D., Yurchuk Yu.S., Lugovtsov A.E., Lin M.D., Priezzhev A.V. *J. Quant. Spectrosc. Radiat. Transfer*, **178**, 315 (2016).
13. Nikitin S.Yu., Ustinov V.D., Tsybrov E.G., Priezzhev A.V. *Izv. Saratov Unive., Novaya Seriya. Ser. Fiz.*, **17** (3), 150 (2017); DOI: 10.18500/1817-3020-2017-17-3-150-157.
14. Nikitin S.Yu., Ustinov V.D. *Quantum Electron.*, **48** (1), 70 (2018) [*Kvantovaya Elektron.*, **48** (1), 70 (2018)].
15. Nikitin S.Yu. *Quantum Electron.*, **48** (10), 983 (2018) [*Kvantovaya Elektron*, **48** (10), 983 (2018)].
16. Bessis M., Mohandas N. *Blood Cells*, **1**, 307 (1975).
17. Hardeman M.R., Goedhart T., Dobbe J.G.G., Lettinga K. *Clin. Hemorheol.*, **14** (4), 605 (1994).
18. Shin S., Ku Y., Park M.-S., Suh J.-S. *Cytometry. Part B (Clinical Cytometry)*, **65**, 6 (2005). DOI:10.1002/cyto.b.20048.
19. Firsov N.N., Dzhanashiya P.Kh. *Vvedenie v eksperimental'nuyu i klinicheskuyu gemoreologiyu* (Introduction to Experimental and Clinical Hemorheology) (Moscow: Izd-vo Rossiiskogo gosudarstvennogo meditsinskogo un-ta, 2004).
20. Nikitin S.Yu., Ustinov V.D., Shishkin S.D. *J. Quant. Spectrosc. Radiat. Transfer*, **235**, 272 (2019); https://doi.org/10.1016/j.jqsrt.2019.07.011.